

Multiscale Coherent Structures and Broadband Waves due to Parallel Inhomogeneous Flows

Valeriy V. Gavrishchaka,¹ Gurudas I. Ganguli,² Wayne A. Scales,³ Steven P. Slinker,² Christopher C. Chaston,⁴
James P. McFadden,⁴ Robert E. Ergun,⁵ and Charles W. Carlson⁴

¹Science Applications International Corporation, McLean, Virginia

²Plasma Physics Division, Naval Research Laboratory, Washington, D.C.

³Bradley Department of Electrical and Computer Engineering, Virginia Polytechnic Institute and State University,
Blacksburg, Virginia

⁴Space Sciences Laboratory, University of California, Berkeley, California

⁵Department of Astrophysical and Planetary Science, Laboratory for Atmospheric and Space Physics, Colorado University,
Boulder, Colorado

(Received 28 June 2000)

Linear theory analysis and particle-in-cell simulations show that a spatial transverse gradient in the ion drift parallel to the magnetic field, $dV_{di}/dx \leq \Omega_i$, where Ω_i is the ion cyclotron frequency, can generate a broadband multimode spectrum extending from $\omega \ll \Omega_i$ to $\omega \gg \Omega_i$. Nonlinearly, these waves lead to multiscale spatially coherent structures, substantial cross-field transport, ion energization, and phase-space diffusion. Large spikes are formed in the parallel electric field time series. These signatures are similar to the Fast Auroral Snapshot satellite observations in the upward current region.

PACS numbers: 94.30.Gm, 52.35.-g

The Fast Auroral Snapshot (FAST) satellite [1] is revealing features of the auroral region with unprecedented accuracy and fine resolution. This has challenged a number of classical notions of the auroral plasma processes and has necessitated a more detailed analysis of the physical processes even at smallest scale sizes in both the upward and downward current regions [2]. Ion beams parallel to the magnetic field along with large amplitude dc electric fields are a hallmark of the upward current region and yet how they influence the dynamics of this region is not clear.

Large electric fields found in the Earth's auroral zone produce shears in the ion flow both parallel and perpendicular to the magnetic field. These shears are observed simultaneously and result from the localized nature of the large, high-altitude, perpendicular electric fields and their equipotential closure at altitudes above the ionosphere. In regions where auroral ion beams form (3000–6000 km), the magnitude of the shear in the ion flow along the magnetic field is typically an order of magnitude larger than its magnitude in the perpendicular flow. At higher altitudes shears in the parallel flow decrease with the magnetic field; however, shears in the perpendicular flow are relatively constant with altitude.

An outstanding issue of significance is the role of the ion beams in the origin of the large-amplitude ion cyclotron waves with their characteristic broadband spectrum, nonlinear ion solitary structures, and double layers which are generally found correlated with these beams [2–4]. This Letter establishes that inhomogeneity in parallel plasma flows, when simultaneously considered with transverse dc electric fields, can reproduce the signatures often observed in the auroral ionosphere especially in the upward current region.

A typical example of FAST high resolution ionospheric observations in the upward current auroral region is

shown in Fig. 1. Figure 1(a) shows the energy spectrum of an ion beam observed close to apogee. The black trace superimposed on the most intense fluxes shows the characteristic energy of the beam which is used to calculate the shear frequency in the ion drift as shown in Fig. 1(b). Assuming a spatial dependence of the observed ion energy, dV_{di}/dx approaches the $1.3\Omega_{O+}$. Shear values up to $5\Omega_{O+}$ have been reported [5]. Figure 1(c) shows the electric field measured along the spacecraft track and approximately perpendicular to the background magnetic field. It shows the existence of intense wave turbulence up to several hundred mV/m spanning the width (under the assumption of stationarity) of the observed ion beam shown in Fig. 1(a). The spectrum of this turbulence shown in Fig. 1(d) indicates mixture of broadband and discrete harmonic features centered on multiples of Ω_{H+} . Close inspection of the time series of the electric field almost parallel to the magnetic field reveals a characteristic spiky waveform as shown in Fig. 1(e). Figure 1(f) presents a slice taken through the dynamic spectrum shown in Fig. 1(d) around the time of the spiky parallel field. The dashed lines are multiples of the proton gyro frequency. Similar features are also observed by other spacecraft [6]; however, the discrete spectral peaks are shifted to above $n\Omega_i$ [7].

To understand this we use a kinetic linear dispersion equation with a uniform magnetic field along the z direction and a nonuniform field-aligned drift $V_d(x)$ [8,9]:

$$1 + \sum_n \Gamma_n(b) F_{ni} + \tau(1 + F_{0e}) + k^2 \lambda_{Di}^2 = 0 \quad (1)$$

where $\Gamma_n(b) \equiv I_n(b) \exp(-b)$, I_n are modified Bessel functions, $b \equiv (k_y \rho_i)^2$, $\tau \equiv T_i/T_e$ is the ion/electron temperature ratio, $k^2 = k_z^2 + k_y^2$, λ_{Di} and ρ_i are ion

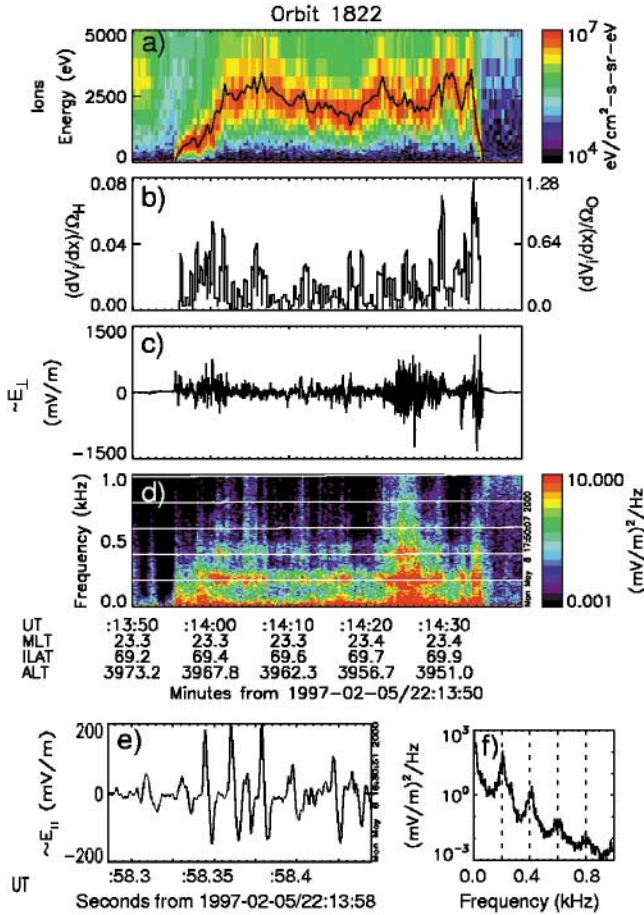


FIG. 1 (color). The ion energy spectrum (a), the shear frequency in the ion drift (b), transverse electric field (c), wave turbulence spectrum (d), time series of the parallel electric field (e), and power spectrum from this time series (f) observed by FAST satellite.

Debye length and gyroradius, respectively, and

$$F_{ni} = \left(\frac{\omega}{\sqrt{2}|k_z|v_{ti}} \right) Z \left(\frac{\omega - n\Omega_i}{\sqrt{2}|k_z|v_{ti}} \right) - \frac{V'_d}{u\Omega_i} \left[1 + \left(\frac{\omega - n\Omega_i}{\sqrt{2}|k_z|v_{ti}} \right) Z \left(\frac{\omega - n\Omega_i}{\sqrt{2}|k_z|v_{ti}} \right) \right],$$

$$F_{0e} = \left(\frac{\omega - k_z V_{de}}{\sqrt{2}|k_z|v_{te}} \right) Z \left(\frac{\omega - k_z V_{de}}{\sqrt{2}|k_z|v_{te}} \right) + \frac{V'_d}{\mu u \Omega_i} \left[1 + \left(\frac{\omega - k_z V_{de}}{\sqrt{2}|k_z|v_{te}} \right) Z \left(\frac{\omega - k_z V_{de}}{\sqrt{2}|k_z|v_{te}} \right) \right],$$

where Z is the plasma dispersion function, $u \equiv k_z/k_y$, $v_{t\alpha}$ is the thermal velocity, $V'_{d\alpha} \equiv dV_{d\alpha}/dx$, and $\mu \equiv m_i/m_e$. We assume that $V'_{di} = V'_{de} \equiv V'_d$ and transform to the ion frame. This allows us to isolate the effects of localized ion beams that prominently feature in the FAST observations in the auroral region [2,3].

We examine the marginal stability condition from (1) in two limits. First, consider $|\omega - n\Omega_i| \ll \Omega_i$, and neglecting shear terms, i.e., $V'_d/u\Omega_i \ll 1$, we get

$$V_{de}^c = \frac{\omega}{k_z} \left[1 + \Gamma_n(b) \frac{\mu^{1/2}}{\tau^{3/2}} \exp\left(-\frac{[\omega - n\Omega_i]^2}{2k_z^2 v_{ti}^2} \right) \right]. \quad (2)$$

This is identical to the homogeneous current driven ion cyclotron instability [10]. The critical drift V_{de}^c increases with the harmonic number n since $\omega \sim n\Omega_i$.

Next, consider the $V'_d/u\Omega_i \gg 1$ limit,

$$V_{de}^c = \frac{\omega}{k_z} - \Gamma_n(b) \frac{(\omega - n\Omega_i)}{k_z} \frac{\mu^{1/2}}{\tau^{3/2}} \frac{V'_d}{u\Omega_i} \times \exp\left(-\frac{[\omega - n\Omega_i]^2}{2k_z^2 v_{ti}^2} \right). \quad (3)$$

Now there is a reduction of V_{de}^c for $\omega \geq n\Omega_i$, for $V'_d/u\Omega_i > 0$. The necessary phase relation for the shear-driven ion-cyclotron modes ($\omega \geq n\Omega_i$) in the absence of any current ($V_{de} = 0$) is

$$\frac{k_y}{k_z} \frac{V'_d}{\Omega_i} > 0. \quad (4)$$

For $\xi = (\omega - n\Omega_i)/k_z \ll 1$ and neglecting higher order ξ terms in Eq. (3), the necessary condition for the critical shear frequency for the n th harmonic is

$$\frac{V'_{dc}}{\Omega_i} > \frac{\beta}{k_y \Gamma_n(b)}, \quad (5)$$

where $\beta = k_z \tau^{3/2} / \mu^{1/2}$ is a constant for a given k_z . Since, to the leading order, the asymptotic limit of the $k_y \Gamma_n$ for large k_y is independent of n , the critical shear values for higher ion-cyclotron harmonics can be close to that of the first harmonic. Thus, for large enough k_y there can be simultaneous growth at many higher ion-cyclotron harmonics for a relatively weak shear. This is in sharp contrast to the homogeneous case where the critical drift for the ion-cyclotron instability increases with n .

Frequency (solid line) and wave number (dashed line) spectra obtained from a linear theory are presented in Fig. 2(a). Here $V_{de} = 0$ (current-free case), $V'_d = 2\Omega_{H+}$, $T_i = T_e$, and $\mu = 1837$. Although multiple harmonics are also unstable for $V'_d \ll \Omega_{H+}$ (especially, when $T_i < T_e$), we consider a larger than typically observed value of shear so that it is relevant to our simulations describing the nonlinear properties. The spectrum is produced by varying k_z and k_y values such that $k_z V_d \ll \Omega_i$ so that a local analysis will be adequate. The frequency spectrum is localized around $\omega = 0$ and $\omega \sim n\Omega_i$ which corresponds to the D'Angelo [11] mode and multiple ion-cyclotron harmonics, respectively. Shear generates modes from $\omega \ll V'_d$ to $\omega \gg V'_d$ along with a very broad wave number band from $k_{\perp} \rho_i \ll 1$ to $k_{\perp} \rho_i \gg 1$. The threshold shear frequencies for higher harmonics are close to each other ($V'_{dc}/\Omega_i = 0.32$ for $n = 1$ to $V'_{dc}/\Omega_i = 0.5$ for $n = 10$), consistent with the scaling argument (5) and they are not sensitively dependent on the mass ratio. The threshold values are found to be significantly lower for $T_i \ll T_e$.

The broadband wave number spectrum allows even small transverse electric field ($|V_E| \equiv c|E/B| \ll v_{ti}$) to

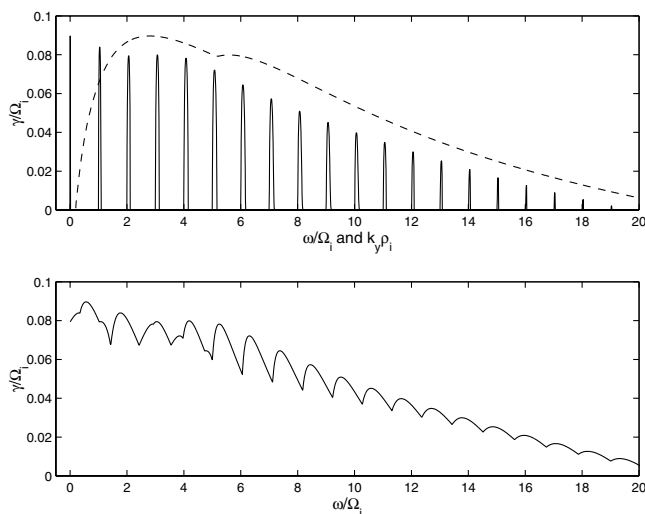


FIG. 2. Frequency (solid line) and wave number (dashed line) spectrums obtained from linear theory for $V_E = 0$ (a) and $V_E = 0.3$ (b). Here $V_{de} = 0$ (current-free case), $V_d' = 2\Omega_{H+}$, $\mu = 1837$, and $\Omega_e/\omega_{pe} = 8.2$. The spectrum is obtained from Eq. (1) by varying k_z and k_y values.

transform the discrete frequency spectrum to a continuous one as usually observed in space [Fig. 1(c)]. This effect is due to a large difference $(\Delta k_y)V_E$ in a frequency Doppler shift experienced by modes. This is illustrated in Fig. 2(b), where a transverse drift with $V_E = 0.3v_{ti}$ is used. The range Δk_y increases with shear magnitude.

Since $\Omega_{H+}/\Omega_{O+} = 16$, the normalized shear frequency $(dV_d/dx)/\Omega_i$ is significantly smaller for the H+ component than for the O+ component. Therefore, while $dV_d/dx \sim \Omega_{O+}$ can generate a continuous spectrum of O+ cyclotron modes over many washed out O+ harmonics, it will generate fewer H+ harmonics with their corresponding Δk_y significantly narrower. This will result in smaller Doppler shift difference that may not be sufficient to wash out the H+ cyclotron structures completely.

The nonlinear properties are investigated by a 2-1/2D electrostatic particle-in-cell (PIC) code with full ion dynamics and gyro-center approximation for electrons [12,13]. To clearly resolve short wavelength modes 900 particles per cell are used and long-wavelength modes are excluded from the present simulation by appropriate choice of the simulation box of $64 \times 16 \Delta$ ($12.5 \times 3\rho_i$) in the (x, y) directions, where grid size $\Delta = \lambda_D = 0.2\rho_i$.

A Maxwellian plasma with $T_i = T_e$, $V_{di} = V_{de} = 0$, and $\mu = 1837$ is initially loaded using standard techniques [12]. The magnetic field is tilted such that $k_z/k_y = 0.01$. After that parallel drift velocities are assigned to ions to obtain inhomogeneous velocity profile as shown in Fig. 3(d) (solid line). The maximum shear frequency is $2\Omega_i$ and the localization scale computed at 1/2 maximum velocity gradient is $3\rho_i$. The maximum shear magnitude used is typical for the observed oxygen species. Lowering this parameter down to that of the hydrogen species ($\leq 0.3\Omega_{H+}$) makes simulations computationally impractical. Piecewise linear loading for gyrocenters is used. For simulation parameters,

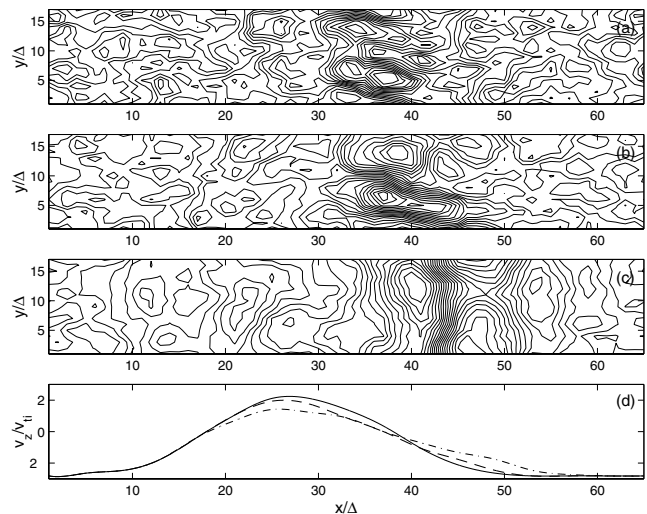


FIG. 3. Electrostatic wave potential obtained from PIC simulations after $\Omega_i t = 40$ (a), 60 (b), 100 (c), and the corresponding ion velocity parallel to the magnetic field (d) shown by solid, dashed, and dot-dashed lines, respectively.

(1) predicts two unstable modes for $k_y \rho_i = 2$ (first simulation mode) and six unstable modes for $k_y \rho_i = 4$ (second simulation mode).

Figures 3(a)–3(c) present wave potential after $\Omega_i t = 40, 60,$ and 100 , and the corresponding parallel ion velocity shown in Fig. 3(d) by solid, dashed, and dot-dashed lines, respectively. The waves are generated in the shear region as required by phase relation (4) for the 2D system which imposes a unique sign of k_z/k_y . Smaller scale coherent structures due to mode 2 appear first, while larger-scale structures due to mode 1 become dominant later. Figure 3(d) also illustrates significant relaxation of the flow gradient due to wave-induced viscosity. Much larger reductions are observed in runs with a larger simulation box that allows longer wavelength modes. The observed values of shear pertain to the steady state, which is much lower than its initial value.

Time series of the spatial Fourier components corresponding to modes 1 and 2 are shown in Figs. 4(a) and 4(b). The structure of the time series as well as spectral analysis indicates that mode 1 is characterized by the D'Angelo mode and the first ion-cyclotron harmonic. Mode 2 is characterized by simultaneous excitation up to five ion-cyclotron harmonics. Combined power spectrum (modes 1 and 2) is shown in Fig. 4(d). This is similar to the observed power spectrum for the H+ cyclotron modes [Fig. 1(e)]. Higher-order Bernstein modes with $\omega \leq \Omega_i$ and finite k_z (e.g., [14]) are also apparent in the simulation. It follows from Eq. (3) that they can also be destabilized by shear.

Figure 4(c) is the time series of the parallel electric field inside the shear region that includes contributions from all possible simulation modes. The simulation time series [Figs. 4(b) and 4(c)] is similar to the observed parallel electric field time series [Fig. 1(e)]. In the simulation, this structure arises when several coherent ion-cyclotron

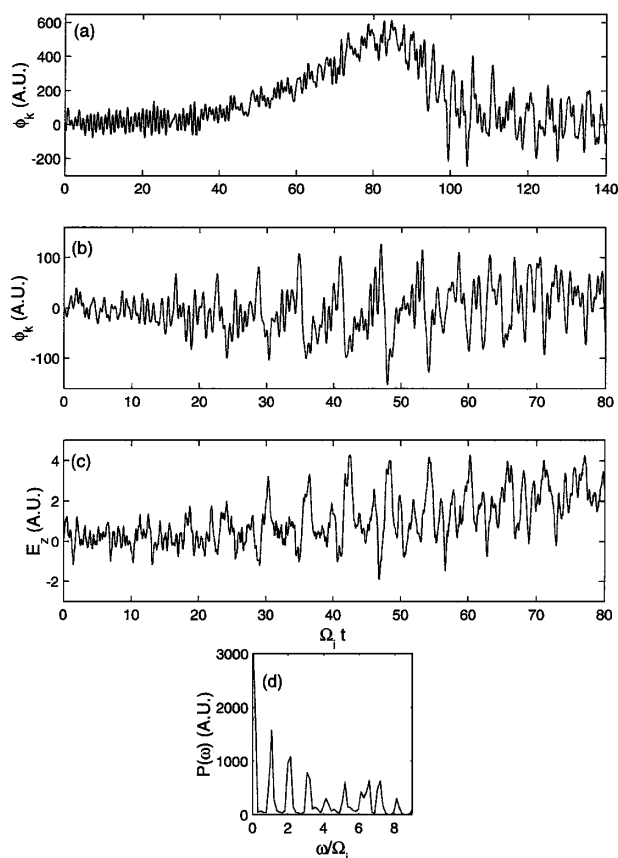


FIG. 4. Time series of the spatial Fourier components corresponding to PIC simulation modes 1 (a) and 2 (b), combined power spectrum (d) for modes 1 and 2, and the time series of the parallel electric field (c) inside the shear region that includes contributions from all possible simulation modes. Mode 1 is characterized by the D'Angelo mode and the first ion-cyclotron harmonic. Mode 2 is characterized by simultaneous excitation up to five ion-cyclotron harmonics.

harmonics are simultaneously excited with comparable amplitudes. As the waves grow and saturate it is found that they lead to considerable ion energization and cross-field diffusion.

It is shown for the first time that inhomogeneous ion flow and/or beams parallel to the magnetic field, in conjunction with the transverse dc electric fields, can generate broadband multimode wave spectrum and associated multiscale spatially coherent structures. The broadband waves lead to ion energization that is consistent with recent observations [6,15]. These physical features are frequently

observed in the auroral ionosphere and they cumulatively define the near-Earth plasma environment. More importantly, the study clarifies the causal sequence of physical events, the knowledge of which is necessary to obtain a predictive capability in this plasma environment, which is of obvious practical importance. This study also highlights the importance of the inhomogeneous nature of the auroral phenomena and the necessity of adequate formalisms to address them. It is also interesting that in the solar plasma environment ion-cyclotron wave dissipation has been recently invoked [16] and it has been argued for quite some time that velocity shear in the parallel flow could play a role in the turbulence arising in this environment [17]. Electromagnetic generalization of the results discussed here may be applicable to the solar plasma environment as well.

Stimulating discussions with J. Penano and P. Schuck are acknowledged. This work is supported by the National Aeronautics and Space Administration and the Office of Naval Research.

-
- [1] C. W. Carlson, R. F. Pfaff, and J. G. Watzin, *Geophys. Res. Lett.* **25**, 2013 (1998).
 - [2] R. E. Ergun *et al.*, *Geophys. Res. Lett.* **25**, 2025 (1998).
 - [3] J. P. McFadden *et al.*, *Geophys. Res. Lett.* **25**, 2021 (1998).
 - [4] M. Temerin *et al.*, *Phys. Rev. Lett.* **48**, 1175 (1982).
 - [5] W. Amatucci, *J. Geophys. Res.* **104**, 14 481 (1999).
 - [6] D. J. Knudsen and J.-E. Wahlund, *J. Geophys. Res.* **103**, 4157 (1998).
 - [7] P. Kintner *et al.*, *J. Geophys. Res.* **84**, 7201 (1979).
 - [8] G. Ganguli *et al.*, *J. Geophys. Res.* **99**, 8873 (1994).
 - [9] V. V. Gavrishchaka, S. B. Ganguli, and G. I. Ganguli, *Phys. Rev. Lett.* **80**, 728 (1998); *J. Geophys. Res.* **104**, 12 683 (1999).
 - [10] J. M. Kindel and C. F. Kennel, *J. Geophys. Res.* **76**, 3055 (1971).
 - [11] N. D'Angelo, *Phys. Fluids* **8**, 1748 (1965).
 - [12] C. K. Birdsall and A. B. Langton, *Plasma Physics via Computer Simulations* (McGraw-Hill, New York, 1985).
 - [13] T. Tajima, *Computational Plasma Physics* (Addison-Wesley, Boston, 1988).
 - [14] D. G. Swanson, *Plasma Waves* (Academic Press, San Diego, 1989).
 - [15] K. R. Lynch *et al.*, *Geophys. Res. Lett.* **23**, 3293 (1996); M. Andre *et al.*, *J. Geophys. Res.* **103**, 4199 (1998).
 - [16] S. R. Cranmer, *Astrophys. J.* **532**, 1197 (2000).
 - [17] D. A. Roberts *et al.*, *J. Geophys. Res.* **97**, 17 115 (1992).